Please cite this article in press as: Ren et al., A semi-automated MEA spike sorting method for high-throughput assessment of cultured neurons, Stem Cell Reports (2026), https://doi.org/10.1016/j.stemcr.2026.102872

STEM CELL REPORTS
Article
ISSCR
OPEN ACCESS

A semi-automated MEA spike sorting method for high-throughput assessment of cultured neurons

Xiaoxuan Ren,[1,2,6] Carissa L. Sirois,[3,4,6] Raymond Doudlah,[4] Ethan E. Dayley,[3,4] Natasha M. Méndez-Albelo,[3,4,5] Aviad Hai,[1,2,*] Ari Rosenberg,[4,*] and Xinyu Zhao[3,4,7,*]
[1]Department of Biomedical Engineering, University of Wisconsin-Madison, Madison, WI 53705, USA
[2]Department of Electrical and Computer Engineering, University of Wisconsin - Madison, Madison, WI 53706, USA
[3]Waisman Center, University of Wisconsin-Madison, Madison, WI 53705, USA
[4]Department of Neuroscience, School of Medicine and Public Health, University of Wisconsin-Madison, Madison, WI 53705, USA
[5]Molecular Cellular Pharmacology Training Program, University of Wisconsin-Madison, Madison, WI 53705, USA
[6]These authors contributed equally
[7]Lead contact
*Correspondence: ahai@wisc.edu (A.H.), ari.rosenberg@wisc.edu (A.R.), xinyu.zhao@wisc.edu (X.Z.)
https://doi.org/10.1016/j.stemcr.2026.102872

SUMMARY

Neurons derived from human pluripotent stem cells (hPSCs) are valuable models for studying brain development and developing therapies for brain disorders. Evaluating hPSC-derived neurons requires assessing their electrical activity, which can be achieved using multi-electrode arrays (MEAs) for extracellular recordings. Because each electrode channel generally detects activity from multiple neurons, resolving the activity of single neurons requires a process called spike sorting. However, currently available methods were not developed for analyzing data from hPSC-derived neurons and require complex workflows and time-consuming manual intervention. Here, we introduce a semi-automated MEA spike sorting software (SAMS) designed specifically for low-density MEA recordings of cultured neurons. SAMS outperforms commercially available automated spike sorting algorithms in terms of accuracy and greatly reduces computational and human processing time. By providing an accessible, efficient, and integrated platform for spike sorting, SAMS enhances the resolution and utility of MEA in disease modeling and drug development using hPSC-derived neurons.

INTRODUCTION

Human pluripotent stem cells (hPSCs) are useful experimental models for defining human-specific biology and disease mechanisms, especially for brain disorders (Niu and Parent, 2020; Sandoval et al., 2024; Zhao and Bhattacharyya, 2018). To evaluate the development and function of hPSC-derived neurons, it is important to assess their electrophysiological properties, particularly their spiking characteristics. Multi-electrode arrays (MEAs) are a widely used tool for simultaneously recording from many neurons *in vivo* (Choi et al., 2021; Guan et al., 2023; Jun et al., 2017; Obaid et al., 2020), *ex vivo* (Zhang et al., 2022), or *in vitro* (Liu et al., 2023; Lv et al., 2023; Spira and Hai, 2013). MEAs detect extracellular field potentials generated by cells proximal to electrodes and have been used to assess the intrinsic properties and network activities of hPSC-derived neurons, allowing for relatively high-throughput assessment of the impact of disease mutations and effects of drug-like compounds (Kiskinis et al., 2014; Liu et al., 2015; Vatine et al., 2017). However, widely used low-density MEA recordings often capture the combined activity of multiple neurons on an individual electrode. To accurately characterize the electrical properties of hPSC-derived neurons, the activities of individual neurons need to be isolated by sorting spikes.

Many spike-sorting pipelines exist for both high-density (electrode spacing <100 μm) and lower-density MEAs (electrode spacing 300–350 μm; Table S1). However, most of these pipelines were created for either *in vivo* recordings or non-human neurons (Carlson and Carin, 2019) and were not optimized for hPSC-derived neurons that have different electrophysiological properties (Cotterill et al., 2016; Hyvärinen et al., 2019; Mayer et al., 2018; Mossink et al., 2021; Napoli and Obeid, 2016). Furthermore, these pipelines require at least some coding skills to run or additional software tools to analyze spike-sorted data. These pipelines thus require time-consuming manual checking and correction of the sorted spikes (McCready et al., 2022; Mehta et al., 2018; Pradeepan et al., 2024; Tyssowski et al., 2019; Vertkin et al., 2015), which limits their application to the analysis of hPSC-derived neurons that contain hundreds of electrodes on a single multi-well plate.

To overcome the challenges of current spike sorting approaches, we developed a semi-automated MEA spike sorting software (SAMS) using low-density MEA data collected from hPSC-derived neurons acquired via the Axion MEA platform. Our goal was to create an open-source end-to-end spike sorting and analysis tool that was user-friendly and accessible to more researchers, especially those without computational expertise. The workflow of SAMS is user interface-based and requires no coding to

Please cite this article in press as: Ren et al., A semi-automated MEA spike sorting method for high-throughput assessment of cultured neurons, Stem Cell Reports (2026), https://doi.org/10.1016/j.stemcr.2026.102872

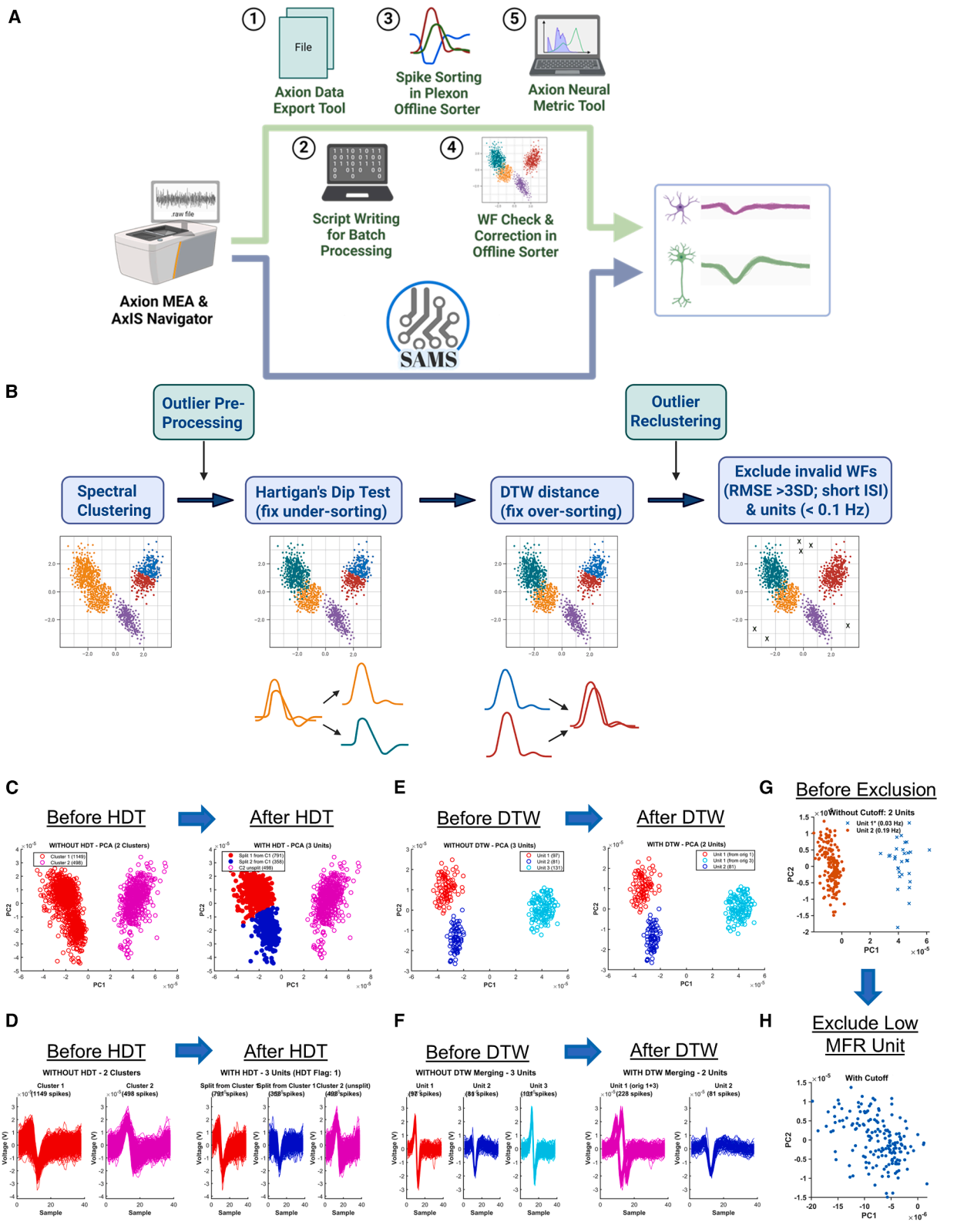

(legend on next page)

implement. Importantly, SAMS flags electrodes that need manual verification, thereby reducing the time needed for analysis. We compared the spike sorting performance of SAMS with Offline Sorter (OFS) software (Plexon, Inc.), the current state-of-the-art software recommended for analyzing low-density Axion MEA recordings. SAMS not only outperformed OFS on spike sorting accuracy, but also decreased the amount of manual validation time. We then used SAMS to reanalyze two previously published MEA datasets of hPSC-derived neurons (Guo et al., 2023; Shen et al., 2023). The SAMS pipeline not only confirmed published conclusions but also uncovered additional differences among experimental conditions. Therefore, SAMS enhances the resolution and utility of MEA recordings in disease modeling and drug development using hPSC-derived neurons.

RESULTS

Overview of spike sorting recommendations for the Axion MEA platform

The recommended pipeline for spike sorting of Axion MEA data involves multiple software tools and manual steps (Figure 1A). First, Axion's AxIS Navigator processes the recordings into spike files, which are converted to NeuroExplorer format using Axion Data Export Tool. Spike sorting using OFS is done one file at a time, through either manual sorting or semi-automated sorting, followed by manual inspection and correction of each sorted electrode channel. Finally, the sorted spikes are analyzed using Axion's Neural Metric Tool, and results are exported. This workflow is time-intensive and requires coding for batch processing. Alternative custom pipelines (Table S1) also require coding proficiency for scripting and were not created for low-density recordings from hPSC-derived neurons.

Overview of spike sorting using SAMS

To address the inefficiencies described above, we developed SAMS as an integrated one-stop platform, enabling automated batch processing of MEA spike files directly into analyzed output results (Figure 1A). SAMS provides an intuitive graphical user interface (GUI) to eliminate the need for scripting while integrating manual spike sorting tools. By consolidating multiple manual steps required for other pipelines, SAMS offers a streamlined workflow to accelerate data processing and analysis. The simplified user experience lowers adoption barriers, enabling scientists without specialized computational skills to readily incorporate high-fidelity information on neuronal encodings into their research.

SAMS employs a multi-step spike sorting pipeline for robust classification (Figures 1B and S1). First, detected spike waveforms are projected onto two principal components. Spectral clustering (von Luxburg, 2007) performs initial unit assignments by testing K = 1–5 clusters and selecting the optimal number using the Davies-Bouldin Index. This unsupervised step maximizes between-cluster variance while minimizing within-cluster variance. Second, outlier waveforms exceeding three standard deviations (SDs) are identified and removed to improve cluster quality (Figures S2A–S2E). Third, Hartigan's Dip Test (HDT) (Hartigan and Hartigan, 1985) assesses unit purity by detecting multimodality in the PCA space of each cluster. Clusters failing HDT are split to correct undersorting (Figures 1C, 1D, and S2F–S2K). Fourth, dynamic time warping (DTW) (Cao et al., 2016) resolves oversorting errors by merging units with similar spike waveform templates (Figures 1E, 1F, and S3A–S3H) based on a user-defined threshold (default: 1.5; Figures S3I–S3M). After a second merge pass to verify cluster assignments, a final step removes invalid waveforms: (1) waveforms exceeding three SDs from each unit's mean template (i.e., averaged waveform), (2) waveforms from low-firing-rate units (default: <0.1 Hz) (Mossink et al., 2021) (Figures 1G and 1H), and (3) waveforms with inter-spike intervals (ISIs) falling within the user-defined refractory period (default: 1.5 ms). By integrating quality control metrics at each step—testing cluster integrity, merging probable oversplits, and removing outliers or false positives—SAMS balances the demands of spike sorting accuracy and manual intervention. The multi-tier workflow maximizes the yield of

Figure 1. Comparison of standard spike sorting workflow and SAMS

(A) Top: standard pipeline for spike sorting of Axion MEA data involving multiple software tools and manual steps. Bottom: pipeline for analysis of Axion MEA data using SAMS, which streamlines the processes shown above by directly interfacing with AxIS Navigator output files and performing automatic batch processing.

(B) Schematic of SAMS processing stages: (1) spectral clustering to perform initial waveform clustering, (2) outlier waveform pre-processing, (3) Hartigan's dip test (HDT) to resolve undersorting, (4) DTW distance calculation to resolve oversorting, (5) outlier reclustering, and (6) exclusion of invalid units and waveforms based on spike frequency criteria and short inter-spike interval (ISI), respectively.

(C–H) PCA plots and waveform traces from analyzed MEA data showing examples of electrodes that were corrected by different stages of the SAMS pipeline.

(C and D) Correction of an undersorted electrode (red) using HDT.

(E and F) Correction of an oversorted electrode (red and cyan in the "Before DTW" images) using DTW distance.

(G and H) Removal of a low-firing-rate unit based on the user-defined threshold (here, 0.1 Hz). See also Figures S2 and S3.

Please cite this article in press as: Ren et al., A semi-automated MEA spike sorting method for high-throughput assessment of cultured neurons, Stem Cell Reports (2026), https://doi.org/10.1016/j.stemcr.2026.102872

high-confidence isolated single units required for revealing biological insights and allows users to customize parameters at each stage of the pipeline to optimize sorting of their data (Table S2). SAMS also returns the parameter settings used for each analysis in the output file to facilitate transparent reporting of methods and to allow users to verify consistent settings between analysis batches.

SAMS provides a user-friendly interface containing key information of output data

To enable users to customize their analyses, SAMS includes panels (Figure 2A) for tuning single-unit burst detection parameters at the single-electrode level (minimum spike count; maximum intra-burst ISI) as well as network burst detection at the multi-electrode level (spike counts, ISIs, and percentage of electrodes participating). While the default parameters are set to be consistent with the defaults applied by AxIS Navigator, which are used by most researchers, the capacity to modify these parameters provides researchers additional flexibility in analyzing their data (Table S2).

SAMS also provides a GUI for manual verification (Figure 2B) and comprehensive output files (Figure 3A). Automated sorting outputs are compiled into a convenient slide deck file (Figure 3B), showing unit assignments, PCA plots, and waveform counts for each electrode. Detailed per-unit metrics are provided in a spreadsheet (Figure 3C), including two lists of flagged electrodes (Figure 3D): the possible multi-unit list (electrodes failing HDT or below the DTW threshold) and the over-excluded unit list (electrodes exceeding the exclusion threshold). Users can reload flagged electrodes into SAMS' manual sorting interface for refinement using click-and-drag selection tools.

SAMS provides consistent performance for spike sorting hPSC-derived neurons

Since the recommended spike sorting tool for data acquired using the Axion platform is Plexon's OFS software (Figure 1A), we benchmarked the performance of SAMS by comparing it to OFS. We first created a "ground truth" spike sorting dataset for comparison (Figures 4A and S4A–S4C) by manually sorting previously published MEA data recorded from dorsal forebrain excitatory neurons derived from one control (CTRL2) and one fragile X syndrome (FXS2) iPSC line (Shen et al., 2023). OFS was used to manually sort waveforms and determine the number of units on each electrode. This ground truth dataset was then used to assess the automated spike sorting performances of SAMS and OFS.

We first evaluated the accuracy of the SAMS pipeline without any manual correction. SAMS correctly sorted more than 70% of electrodes in both CTRL2 and FXS2 conditions (Figure 4B). Among incorrectly sorted electrodes, most were errors of undersorting (17.5%–20.3%), with oversorting being less frequent (6.0%–9.7%). Next, we compared SAMS to the four algorithms offered by OFS. We first ran each algorithm using default settings, then ran them several more times after adjusting one or more parameters. The settings with the highest pooled accuracy are shown in Figures 4C–4F, and accuracy values for each batch across different algorithms are shown in Figures 4G and 4H (see also Figures S4D–S4G; Table S3). Among the OFS algorithms, T-Dist EM achieved the highest accuracy (Figures 4C, 4G, and 4H), with accurate sorting of up to 43.8% of FXS2 and up to 64.5% of CTRL2 electrodes. Although 64.5% is within acceptable accuracy ranges, and in some cases similar to the accuracy achieved by SAMS, the T-Dist EM Scan algorithm exhibited high variability between batches of the same condition (6.9%–88.9% for CTRL2; 1.2%–77.8% for FXS2), while SAMS performed more consistently for all neurons from both FXS2 and CTRL2 conditions (67.4%–94.4% for CTRL2, 62.9%–80.2% for FXS2; Figures 4G and 4H). The other three OFS algorithms performed worse than T-Dist EM Scan (Figures 4D–4F), with none achieving more than 42.9% correct sorting (Figures 4G and 4H). In addition, SAMS consistently achieved lower levels of oversorting than the OFS algorithms (Figures S4D and S4E), while errors of undersorting were similar across all platforms and algorithms (Figures S4F and S4G). Therefore, SAMS, which was developed specifically for sorting hPSC-derived neuron data, consistently achieved accuracy levels comparable to spike sorting methods used to analyze *in vivo* or simulated MEA datasets (Buccino et al., 2020; Mohammadi et al., 2024; Souza et al., 2019; Wang et al., 2023).

Correction of electrodes flagged by SAMS can further improve accuracy

A major challenge in performing spike sorting of MEA data recorded from hPSC-derived neurons is the sheer volume of electrodes to be sorted, because it is necessary to assess not only multiple hPSC lines, but also multiple batches of neurons derived from each hPSC line to minimize both biological and technical variabilities (Anderson et al., 2021). For example, weekly recording of one 96-well plate from Axion for 8 weeks produces data from 6,144 electrodes.

Even though SAMS offers acceptable accuracy levels, users may want to achieve higher accuracy levels than those produced by automatic sorting alone. To help strike a balance between the improved accuracy offered by manual electrode correction after automatic sorting and reduced labor, SAMS returns two lists of electrodes flagged by the algorithm as possibly being incorrectly sorted in each output file (Figure 3D). Manual correction of only flagged electrodes in FXS2 and CTRL2 datasets improved

Figure 2. SAMS graphical user interfaces and features

(A) SAMS graphical user interface (GUI) for automatic batch spike sorting, which includes (1) file selection; (2) spike sorting parameter adjustment (Table S2); (3) single-unit burst detection parameters; (4) electrode-level network burst detection parameters; and (5) progress indicator.

(B) SAMS GUI for manual correction of spike sorting results, which includes (1) data file selection; (2–4) parameter adjustments (same as in A); (5) electrode selection; and (6) correction tools. Data shown are for illustrative purposes.

Please cite this article in press as: Ren et al., A semi-automated MEA spike sorting method for high-throughput assessment of cultured neurons, Stem Cell Reports (2026), https://doi.org/10.1016/j.stemcr.2026.102872

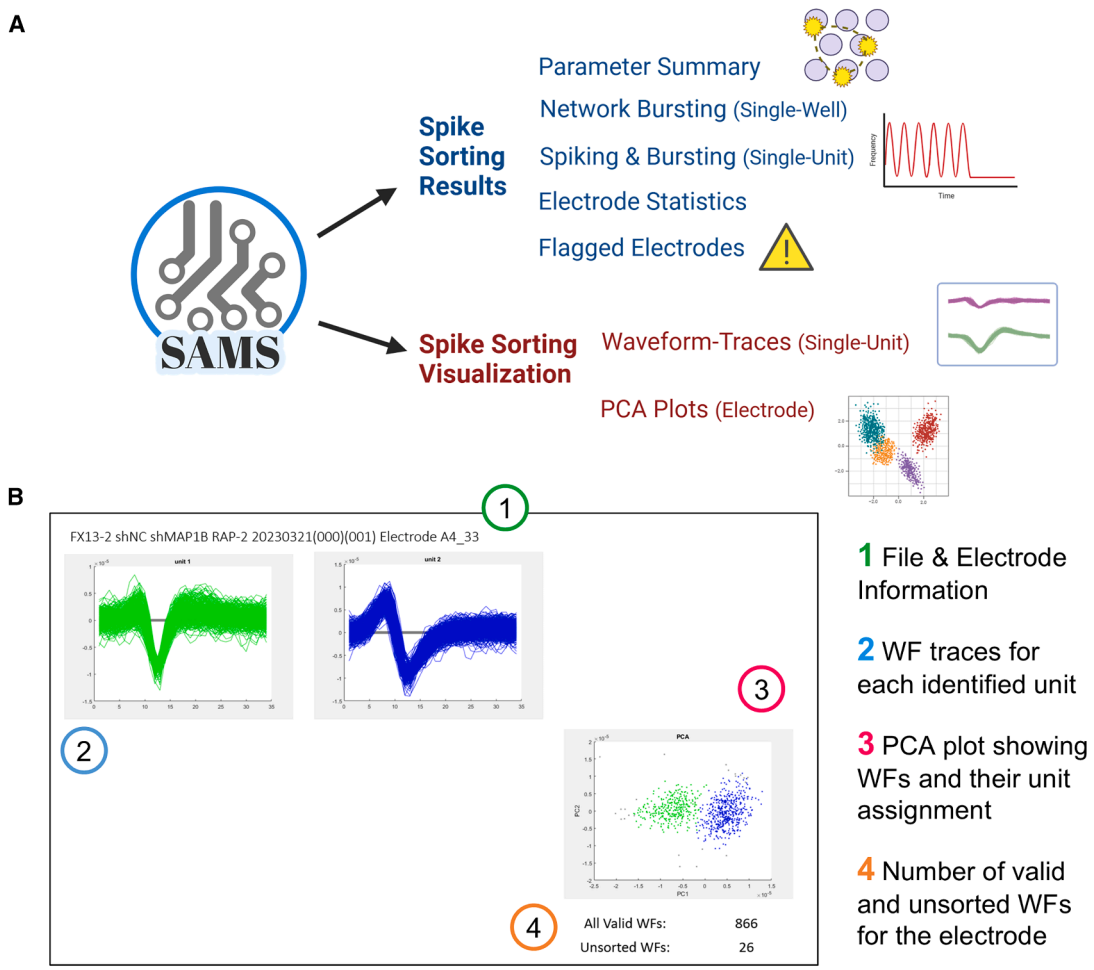

C

	A	B
1		parameter Value
2	threshold_to_merge	1.5
3	refractoryT	0.0015
4	min_spikes_E	5
5	max_ISI_E	100
6	min_spikes_N	50
7	max_ISI_N	100
8	network_participation_threshold	0.35
9	cutoff_frequency	0.1
10	flag_threshold	0.2
11	std_cutoff	3
12	overlap_threshold	0.7

D

	A	B	C
1	Possible MultiUnit	over-exlcuded unit	
2	A2_11	A6_13	
3	A3_11	A9_33	
4	A4_12	A11_21	
5	A5_33	B6_31	
6	A6_33	B9_31	
7	A7_11	C3_33	
8	A7_13	C7_21	
9	A7_23	C8_12	
10	A7_33	C8_13	

Figure 3. Output files for comprehensive spike sorting

(A) Schematic illustrating SAMS data and outputs.

(B) Electrode-specific spike sorting results are saved in a Powerpoint slide deck. Each slide presents sorting outcomes for an individual electrode (1), displaying color-coded waveforms of defined units (2) alongside corresponding Principal-component analysis (PCA) plot (3)

(legend continued on next page)

the accuracy by 2.0%–8.3% (Figure S5A as compared to Figures 4B and S5B–S5F).

SAMS is highly accurate in analyzing various recording conditions

Longer recordings generate more data points and increase analytical burden, while shorter recordings can affect MEA data consistency (Negri et al., 2020). Therefore, we first assessed whether recording time impacted the performance of SAMS. The human-machine consistency (HMC) remained high (mean: 68.6%–70.8%) and stable across recording durations of up to 15 min for both FXS2 and CTRL2 neurons (Figures 5A and S6A). Figure 5B provides a detailed view of electrode-specific performance across recording durations, revealing patterns of electrodes that were consistently accurately sorted (cyan) compared to our ground truth dataset and those requiring manual correction (red). These results reflect the increase in accurately sorted electrodes indicated by the results in Figure 5A and also show that certain electrodes are difficult to resolve independent of recording duration. Because hPSC-derived neurons continue to mature *in vitro* after plating (Cotterill et al., 2016; Hruska-Plochan et al., 2024; Lemieux et al., 2024; Mossink et al., 2021); we also examined whether the culturing time affected the performance of SAMS (Figure S6F). Here, HMC remained relatively stable (60.7%–100%) between 6 and 8 weeks of culture (Figures 5C and 5D). Therefore, SAMS exhibited high accuracy regardless of the developmental stage of the neural network.

We next asked whether the accuracy of SAMS was related to the number of recorded spikes by plotting the percentage of correctly sorted units (Figure 5E) or electrodes (Figure S6B) as a function of total spike count. The majority of units (87.5%) in the entire dataset (both FXS2 and CTRL2) did not exceed 10,057 spikes over the 15-min recording duration (~11.2 Hz), and accuracy up to this spike count remained at or above 70.2%. We did observe a decrease in accuracy for units and electrodes that had greater than 10,057 spikes, although cells with firing rates at these levels were less common in our dataset. For users aiming to analyze datasets with a larger number of cells with such high firing rates, we strongly suggest that they empirically tune the parameter settings for SAMS to maximize accuracy for that higher range.

Motivated by our findings, and because FXS neurons tend to exhibit higher spike counts than control neurons (Shen et al., 2023), we decided to compare the accuracy of SAMS between the two conditions (Figure S6C). To assess this, Kendall's Tau was selected as a non-parametric measure of ordinal association, and significance was tested for (a) all electrodes, (b) only FXS2, and (c) only CTRL2 conditions (Figure S6D). For all three conditions, there was a significant, monotonic negative association between SAMS performance and the number of spikes. These findings indicate that there is a modest decrease in the performance of SAMS at higher spike counts, although the accuracy achieved at these higher spike counts is still within an acceptable range. We further tested whether SAMS performed differently by condition (FXS2 vs. CTRL2) by using a bootstrapped 95% confidence interval of the proportion of electrodes accurately sorted by SAMS. This confidence interval (−0.0812, 0.0894) contained 0 (no group difference), indicating that there was no significant difference in SAMS performance between FXS2 and CTRL2.

Finally, we wanted to test the robustness of SAMS by analyzing more diverse MEA recording datasets. Since SAMS was developed using neurons differentiated using a dual SMAD-inhibition protocol (Shen et al., 2023), we next assessed whether SAMS could be used to analyze neurons generated through Neurogenin 2 (*NGN2*)-directed differentiation, as these neurons can exhibit different temporal trajectories in their differentiation and maturation (Hulme et al., 2022; Lin et al., 2021; Rosa et al., 2020). First, we examined the accuracy of SAMS in sorting neurons from iPSCs derived from an ASD patient with 5q13.2 triplication (Guo et al., 2023) Compared to the ground truth data obtained by manual spike sorting in OFS (Figure 4A), SAMS averaged 83.4% accurate sorting of electrodes across the three batches of neuronal differentiation (Figure S6E). We next assessed the performance of SAMS on a single batch of MEA data from *NGN2*-induced neurons recorded from 12 to 23 days *in vitro* by another laboratory (Afshar-Saber et al., 2024b). These iPSCs were derived from a patient with a homozygous *ALDH5A1* mutation (Proband), the patient's mother (Mom), who is a carrier for the mutation, and a CRISPR-corrected isogenic control line (isoCTRL) (Afshar-Saber et al., 2024a). We observed consistent accuracy in spike sorting by SAMS over the duration of the time course for all three conditions, with only one time point from one of the cell lines falling below 75.6% accuracy (Figures 5F and 5G). These accuracy values (65.5%–100%) were also similar to the accuracy values achieved for our datasets (Figures 4B and S6A).

and quantification of valid and invalid waveforms (WFs; 4). This visualization facilitates rapid assessment of automatic sorting quality and aids in identifying potential sorting errors.

(C) Parameter list: summary of parameter settings used for automated spike sorting.

(D) Quality control: list of potentially missorted electrodes flagged by SAMS, enabling targeted manual refinement of sorting results.

Please cite this article in press as: Ren et al., A semi-automated MEA spike sorting method for high-throughput assessment of cultured neurons, Stem Cell Reports (2026), https://doi.org/10.1016/j.stemcr.2026.102872

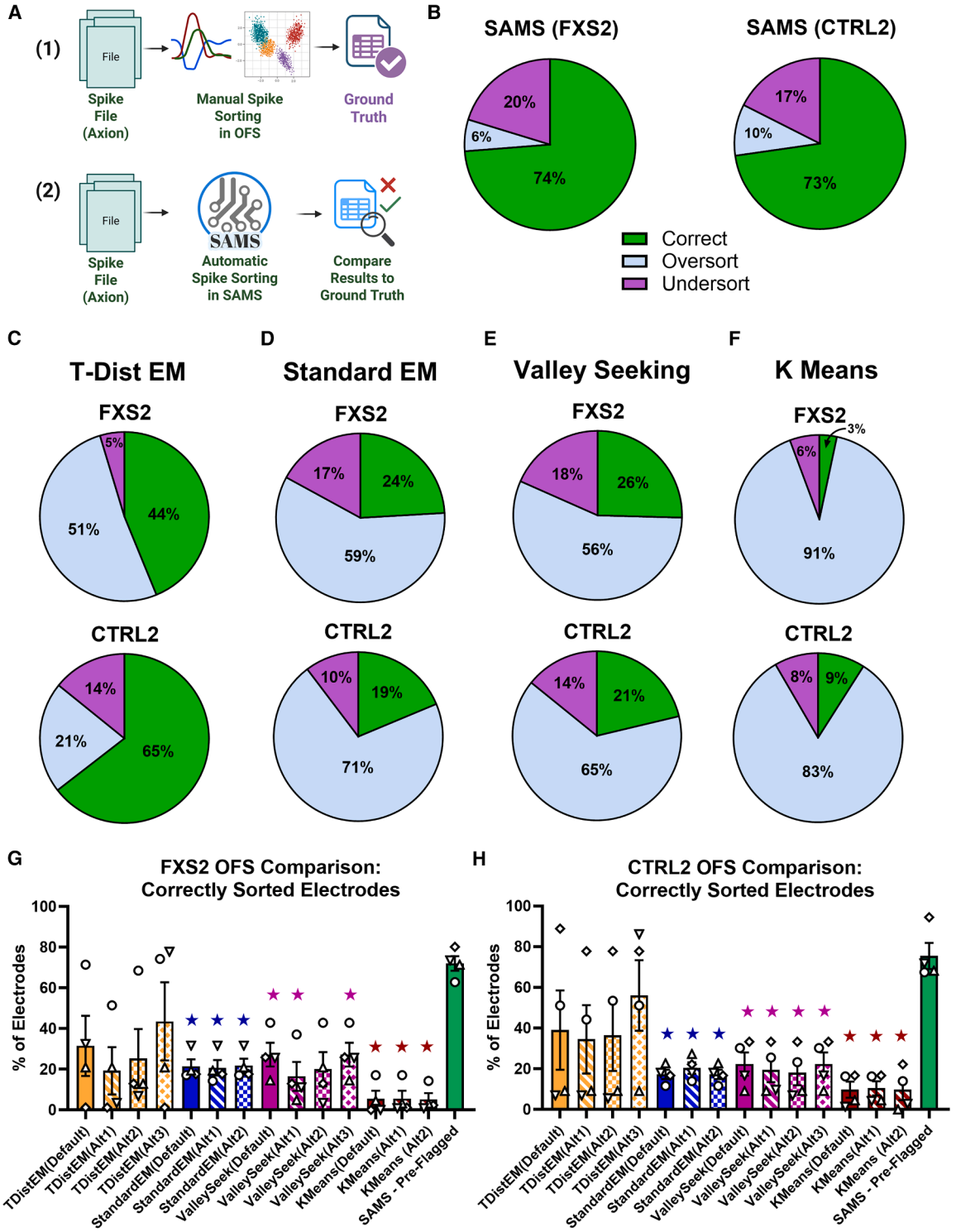

Figure 4. Comparison of SAMS and OFS automatic sorting algorithms

(A) Schematic summarizing (1) ground-truth establishment of MEA data using OFS and (2) comparison of SAMS with ground truth data.

(B) Mean of SAMS without manual correction of any electrodes in FXS2 (left) and CTRL2 (right) neurons.

(C–F) Highest mean accuracy achieved using automated spike sorting algorithms available in OFS software for FXS2 (top) and CTRL2 (bottom) neurons. (C) TDistEM: T-Dist E-M Scan; (D) StandardEM: Standard E-M Scan; (E) ValleySeeking: Valley Seeking Scan; (F) KMeans: K-Means Scan.

(legend continued on next page)

These results collectively indicate that SAMS provides robust and accurate spike sorting across various recording conditions and spike characteristics, with particular strengths in handling lower amplitude signals and moderate spike counts. The algorithm's performance remains consistent across the different maturation stages of neuronal cultures.

Using SAMS to assess electrical activity changes in human neurons with autism-related mutations

To evaluate SAMS as a tool for improving resolution in assessing phenotypes of neurons derived from patients, we next analyzed our published MEA data that had not been subjected to spike sorting. We first examined the activity in neurons that had been differentiated from a pair of FXS (FXS1) and CTRL (CTRL1) hPSCs using *NGN2* induction (Guo et al., 2023). We found that SAMS achieved around 80.5% accuracy for CTRL1 neurons (Figure 6A) and 63.0% accuracy for FXS1 neurons (Figure 6B). We previously reported that FXS1 hPSC-derived neurons exhibit higher mean firing rate (MFR) than CTRL1 neurons, but do not exhibit differences in burst frequency, and that the elevated MFR in FXS1 neurons can be reduced by knocking down *MAP1B* (Figure 6C) (Guo et al., 2023). SAMS analysis confirmed our published results (Figures 6C–6E). Importantly, SAMS resolved an additional difference among experimental conditions: knocking down *MAP1B* in FXS neurons significantly decreased burst frequency at the single-unit level (Figure 6C).

We additionally examined the activity of CTRL hPSC-derived neurons (CTRL3) and hPSC-derived neurons with elevated *MAP1B* (MAP1B-EE) expression differentiated using *NGN2* induction (Guo et al., 2023). We observed significantly increased burst frequency and number of bursts, and no difference in burst duration, which is consistent with our published MEA analysis without spike sorting (Figures S7A–S6C).

We lastly returned to our FXS2 and CTRL2 neurons differentiated using dual SMAD inhibition (Shen et al., 2023). The differences between CTRL2 and FXS2 neurons observed using SAMS, without manual correction, were consistent with the results obtained using standard MEA analysis (Figures 6F–6H; Table S4). SAMS was also able to resolve differences in burst duration and inter-burst interval (Figures S7D–S7I), as well as in other bursting parameters (Table S4), that did not reach statistical significance using standard MEA analysis methods.

We last wanted to confirm whether sorting of spikes into individual units, and the removal of low-activity or outlier waveforms, influenced the electrode level network activity, as SAMS combines the single-unit data for each electrode and then calculates electrode-level network activity parameters from this recombined data. We again observed consistent differences in the network activity between FXS2 and CTRL2 neurons as we did with standard MEA analysis (Figures S7J–S7N; Table S4), including a change in statistical significance for the network burst duration (Figures S7L–S7N). Together, SAMS not only yielded consistent results as the standard MEA analysis but also identified an additional electrophysiological feature that was previously missed.

SAMS allows for separate analysis of bursting and non-bursting neurons from each electrode

Finally, we wanted to utilize SAMS to better understand our neuronal populations. For spiking parameters such as mean firing rate, standard MEA data analysis combines firing rates from neurons that exhibit bursting activity with those neurons that do not. As differences in bursting activity can be due to differences in electrical maturation or other neuronal properties (Hulme et al., 2022; Li et al., 2020; Lin et al., 2021), and bursting differences have been observed in hPSC-derived neuron models of neurodevelopmental and neuropsychiatric disorders (Afshar-Saber et al., 2024b; Amatya et al., 2019; Guo et al., 2023; Que et al., 2021; Shen et al., 2023; Tidball et al., 2020), spike sorting can enable the user to make direct comparisons of neurons that are, for example, more similar in their electrical maturity. Although the increase in MFR in spike-sorted MAP1B-EE neurons did not reach statistical significance, there were significantly higher firing rates in bursting MAP1B-EE neurons compared to bursting CTRL3 neurons (Figure 7A). This finding is particularly interesting given there was no significant difference in the proportion of CTRL and MAP1B-EE neurons that exhibited bursting activity and that 93.2%–99.5% of neurons exhibited bursting activity in each batch of neurons (Figure 7B).

FXS neurons exhibit overall hyperexcitability compared to control neurons, with increased rates of spiking and bursting (Das Sharma et al., 2020; Gildin et al., 2022; Graef et al., 2020; Guo et al., 2023; Liu et al., 2018; Shen et al., 2023). Different genetic or pharmacological interventions to ameliorate these *in vitro* FXS phenotypes decrease overall firing rates but can have varying effects on bursting or network activity (Guo et al., 2023; Shen et al., 2023).

(G and H) Percentage of all electrodes that were accurately sorted by the indicated algorithm in FXS2 (G) and CTRL2 (H) neurons. Data shown are from $n = 4$ independent neuronal differentiations (B1–B4) of $N = 1$ iPSC line per condition. Batches are represented by different symbol shapes. Statistics: (G and H) Data shown as mean (± SEM). Brown-Forsythe & Welch's ANOVA tests with Dunnett's T3 post-hoc correction for multiple comparisons. ★ significant difference compared to SAMS. See also Figures S4D–S4G and Table S3.

Please cite this article in press as: Ren et al., A semi-automated MEA spike sorting method for high-throughput assessment of cultured neurons, Stem Cell Reports (2026), https://doi.org/10.1016/j.stemcr.2026.102872

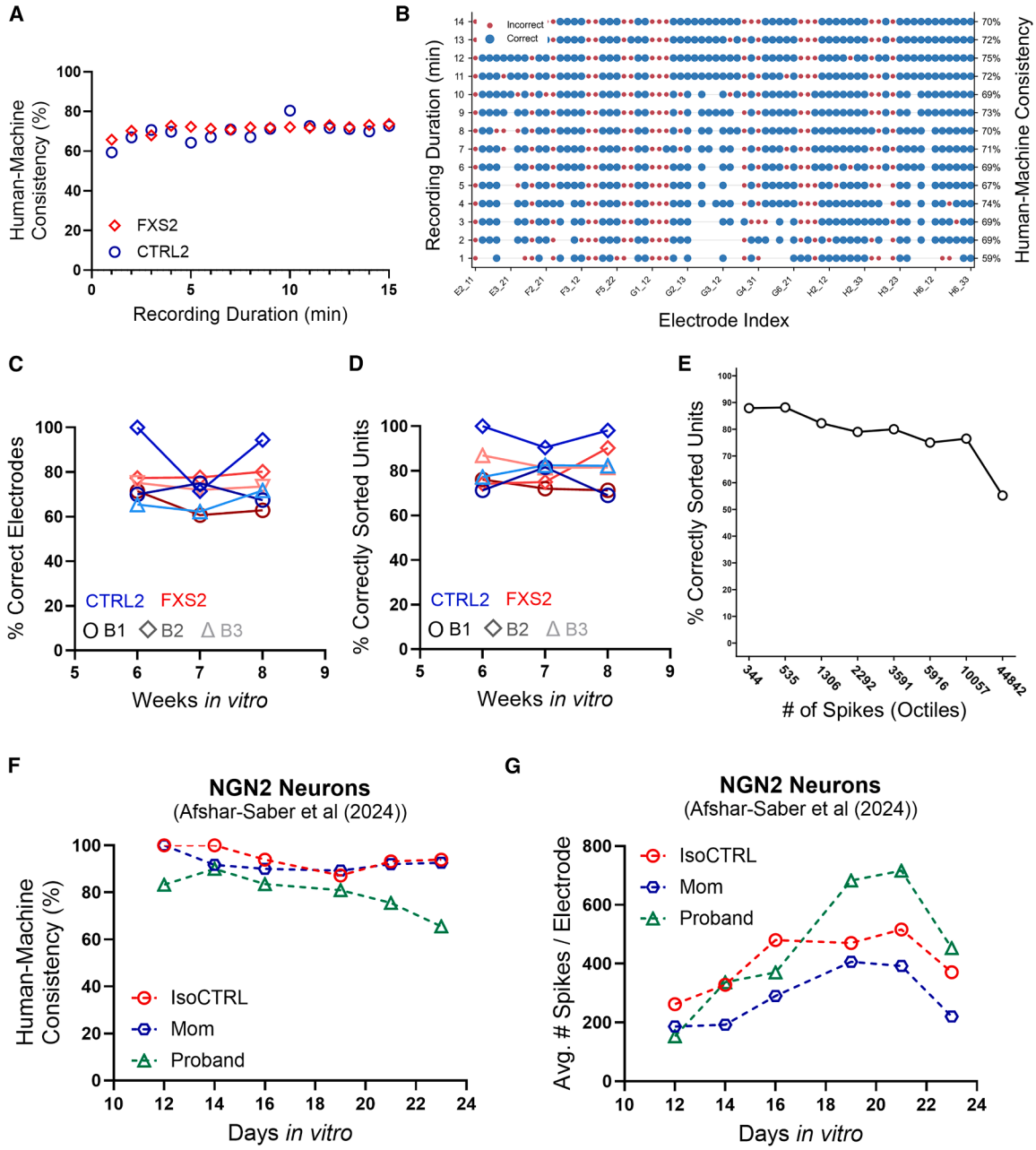

Figure 5. Factors affecting human-machine consistency

(A) Human-machine consistency (HMC; percentage of total electrodes that were accurately sorted) over recording duration length for FXS2 and CTRL2 neurons. Consistency remains above 65% for ≥6-min recording durations. See also Figure S6A.

(B) Electrode-specific HMC (right ordinate) across different recording durations (left ordinate), showing that recording duration does not dramatically impact sorting accuracy on the single-electrode level. Data shown are from CTRL2 neurons at 8 weeks *in vitro*. Cyan: correctly sorted, red: incorrectly sorted.

(C and D) HMC, shown as the percentage of accurately sorted units (C) or electrodes (D), across time of neuronal culturing (6–8 weeks *in vitro*) for FXS2 and CTRL2 neurons. Each batch is represented as a different shape and color. See also Figure S6F.

(E) Percentage of correctly sorted units (both FXS2 and CTRL2) relative to total number of spikes per electrode, split into octiles. See also Figures S6B–S6D. Data in (A and E) are from $n = 4$ independent neuronal differentiations (B1–B4) of $N = 1$ iPSC line per

(legend continued on next page)

Neurons derived from two FXS and two control individuals (FXS1, FXS2, CTRL1, and CTRL2) exhibited increased firing rates as determined using standard MEA analysis (Guo et al., 2023; Shen et al., 2023) or when the single unit activity from both bursting and non-bursting neurons was combined into one group (Figures 6E and 6G). Both sets of FXS neurons that exhibited bursting activity had increased firing rates compared to their respective controls (Figures 7C and 7F). Interestingly, non-bursting FXS1 neurons had similar firing rates as the non-bursting CTRL1 neurons (Figure 7D), while non-bursting FXS2 neurons actually had decreased firing rates compared to CTRL2 (Figure 7G). Additionally, while the proportion of neurons that exhibited bursting activity was higher in both FXS lines, this difference was significant only in FXS2 neurons (Figures 7E and 7H).

Knockdown of the *MAP1B* gene using shRNA partially rescued FXS1 MEA phenotypes both without spike sorting (Guo et al., 2023) and after spike sorting by SAMS (Figure 6D). Interestingly, SAMS revealed that while knockdown of *MAP1B* did not significantly alter the firing rates of bursting FXS1 neurons, there was no longer a statistically significant difference compared to CTRL1 bursting neurons (Figure 7C). Moreover, there was a significant increase in the firing rates of non-bursting FXS1 neurons following *MAP1B* knockdown (Figure 7D) and in the proportion of FXS1 neurons that exhibited any bursting activity (Figure 7E). Together, these results demonstrate the effectiveness of SAMS in enhancing the resolution of MEA data and revealing novel insights when comparing hPSC-derived neurons across conditions.

DISCUSSION

SAMS represents a significant advancement in spike sorting of low-density MEA recordings, particularly hPSC-derived neurons. By integrating multiple algorithms and quality control measures, SAMS addresses several key challenges in the current spike sorting landscape. First, SAMS significantly streamlines the spike sorting workflow. The traditional pipeline, involving multiple software programs and file formats, and extensive manual intervention, is time-consuming and requires specialized coding skills for bulk processing. SAMS consolidates these steps into a single, user-friendly interface, making advanced spike sorting techniques accessible to a broader range of researchers. This democratization of spike sorting technology has the potential to accelerate neuroscience research, particularly *in vitro* disease modeling using hPSC-derived neurons. As the field of neuroscience continues to generate increasingly complex datasets, tools like SAMS will play a crucial role in extracting meaningful insights from neural recordings, ultimately contributing to our understanding of brain function and dysfunction.

The performance of SAMS, which was designed and optimized using hPSC-derived neuron data, was more consistent than the automated sorting algorithms of OFS. This is not surprising given that OFS was designed and optimized for spike sorting of *in vivo* recordings since *in vitro* hPSC-derived neuron recordings differ dramatically from *in vivo* recordings in features such as signal-to-noise ratio. In particular, spike files generated using the recommended default AxIS Navigator settings appear particularly susceptible to oversorting as a result of triggering spike detection with both positive and negative thresholds. Our analysis shows that SAMS achieves relatively high human-machine consistency (mean accuracy: 80.2% (range: 60.7%–100%)) across various recording durations, neuronal culture maturities, batches of neurons, and neurons from different hPSC lines or disease conditions. These levels of accuracy are on par with, or exceed, current-state-of-the-art algorithms that have been developed for spike sorting of MEA data acquired from other platforms or tissue types (Buccino et al., 2020; Mohammadi et al., 2024; Pradeepan et al., 2024; Souza et al., 2019; Wang et al., 2023), and this robustness is crucial for ensuring reliable results across diverse experimental paradigms. The ability of SAMS to maintain performance across different maturation stages of neuronal cultures is particularly valuable for developmental studies, long-term experiments, and repeated recordings of the same neurons over weeks in culture.

Regarding whether this improved performance reflects reduced neuronal overlap rather than algorithmic robustness: low-density arrays do present fewer overlapping waveforms per electrode, which simplifies certain aspects of spike sorting. However, our algorithm was specifically designed as a tool to address the challenges common to these recordings, including similar waveform shapes across units, burst detection, and noise contamination. The consistent performance across multiple culture types, recording conditions, and developmental stages within our dataset suggests that the improvements are not solely attributable to signal sparsity.

condition. Data in (C and D) are mean ± SEM from $n = 3$ independent neuronal differentiations (B1–B4) of $N = 1$ iPSC line per condition.

(F and G) SAMS performance over 11 days *in vitro* (DIV) using an external dataset of MEA recordings from $n = 1$ batch of *NGN2*-induced neurons from a patient with homozygous *ALDH5A1* genetic variant (Proband), as well as from an isogenic CRISPR-engineered heterozygous line (IsoCTRL) and from the patient's mother (Mom).(Afshar-Saber et al., 2024b). See also Figure S6.

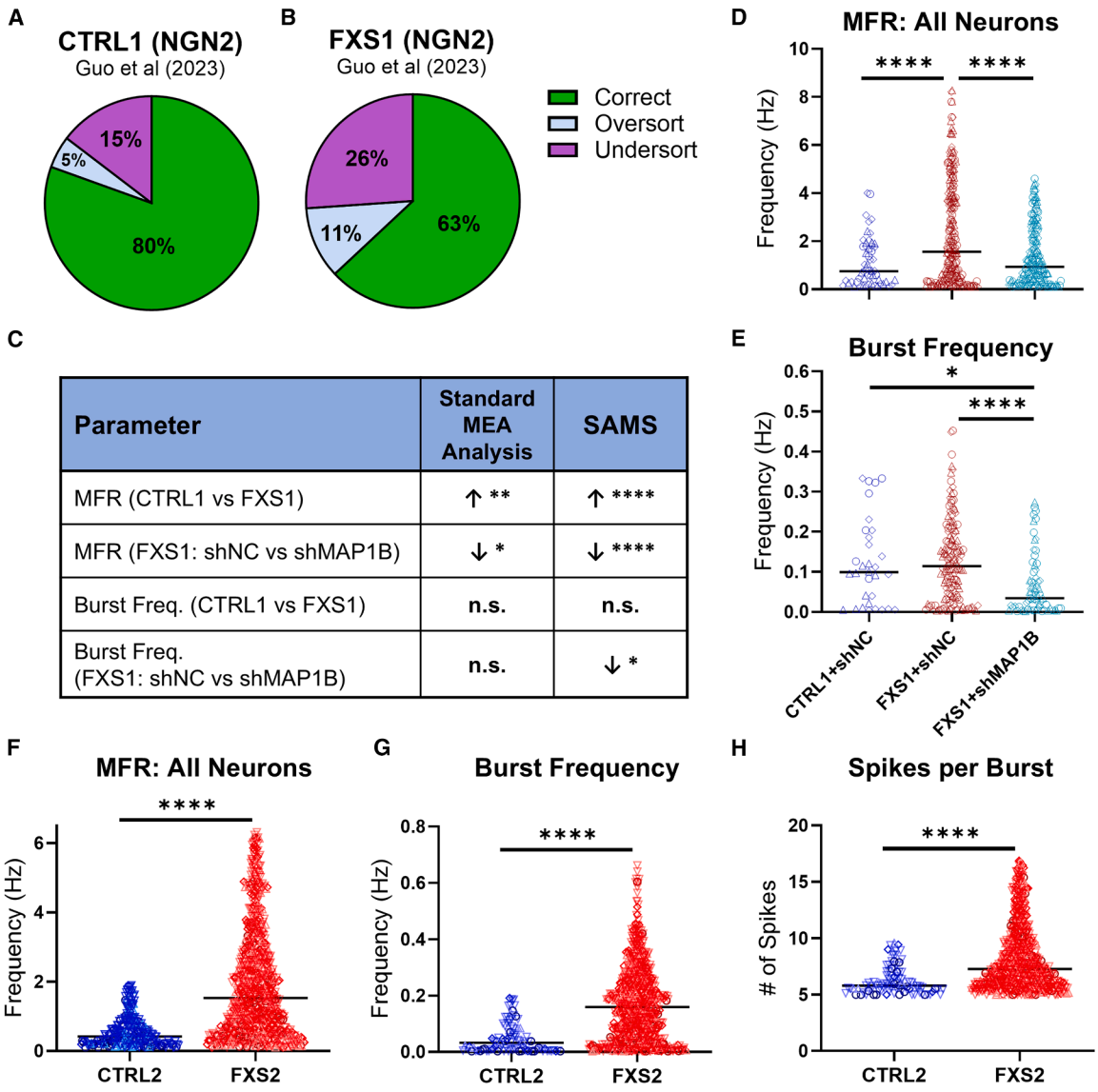

Figure 6. Comparison of SAMS findings to published bulk MEA analysis results

(A and B) Mean accuracy of SAMS in sorting CTRL1 (A) and FXS1 (B) data from (Guo et al., 2023). $n = 3$ independent batches of neurons (B1–B3) from $N = 1$ iPSC line per group.

(C) Summary of results for the two parameters reported in Guo et al. and following analysis of the same data by SAMS.

(D) Mean firing rate (MFR) and (E) burst frequency in CTRL1+shNC, FXS1+shNC, and FXS1+shMAP1B neurons after performing spike sorting with SAMS. $n = 3$ independent batches of neuronal differentiation per condition (D: $n = 56–232$ individual neurons; E: $n = 32–150$ individual neurons).

(F–H) Results from spike sorting of data from (Shen et al., 2023). (F) Mean firing rate, (G) burst frequency, and (H) number of spikes per burst in CTRL2 and FXS2 neurons. $n = 4$ independent batches of neuronal differentiation (B1–B3 and B5). (F) $n = 251$ (CTRL2), 759 (FXS2) neurons; (G) $n = 94$ (CTRL2), 720 (FXS2) neurons; (H) $n = 92$ (CTRL2), 619 (FXS2) neurons. Batches are represented by different symbol shapes. See also Figure S7. Statistics: (D and E) Brown-Forsythe & Welch's ANOVA with Dunnett's T3 correction for multiple comparisons; (F–H) Welch's t test. $^{*}p < 0.05$, $^{****}p < 0.0001$.

The multi-step approach employed by SAMS—combining spectral clustering, HDT, DTW, and waveform validation—provides a comprehensive tool to help deal with common spike sorting issues by compensating for the limitations of individual spike sorting algorithms. This approach effectively addresses both undersorting and oversorting problems, maintaining a balance between sensitivity and specificity in unit identification. The levels of accuracy achieved

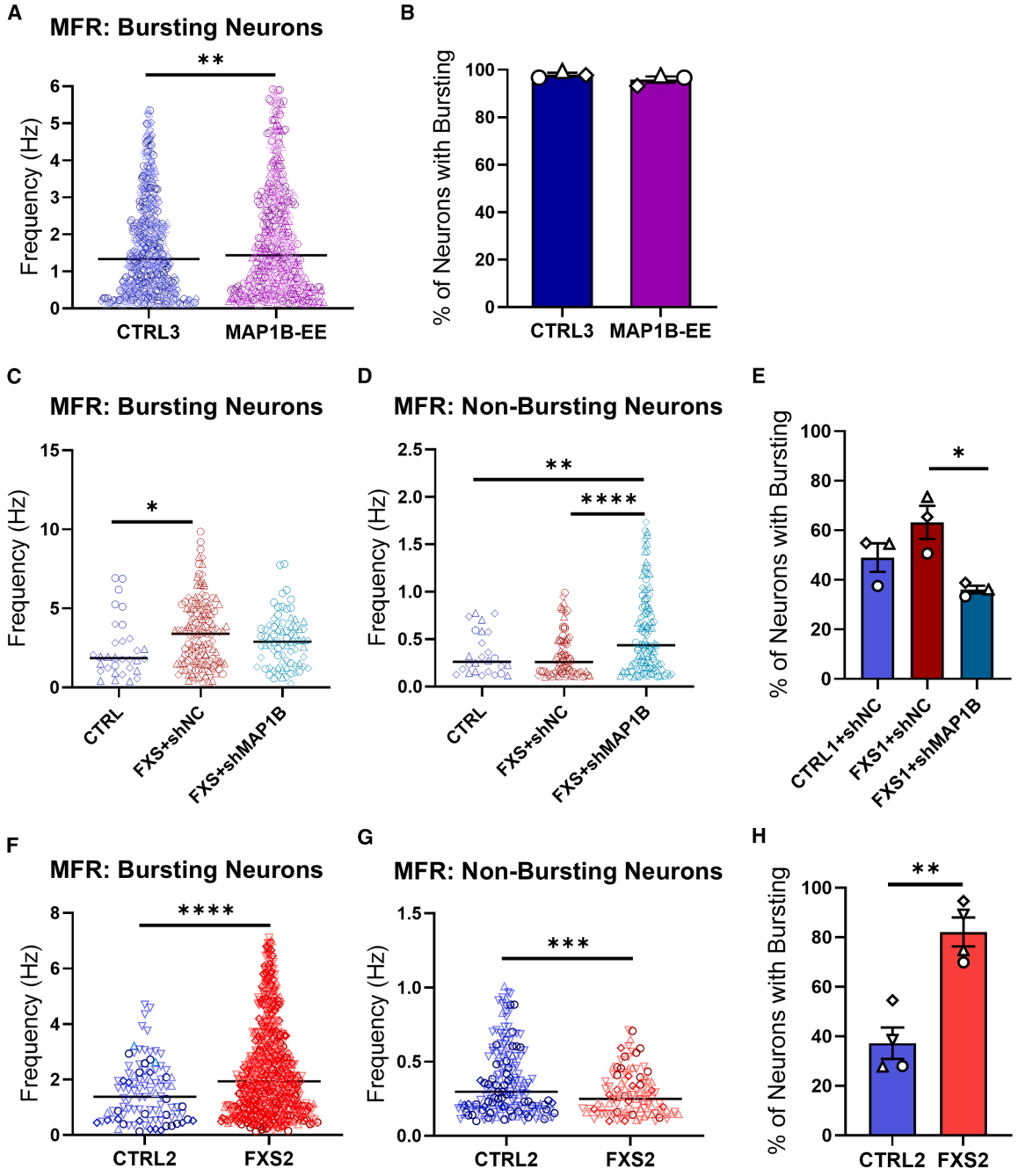

Figure 7. Examination of bursting and non-bursting neuronal populations using SAMS

(A–E) Data from (Guo et al., 2023).

(F–H) Data from (Shen et al., 2023).

(A, C, and F) Mean firing rate in neurons that exhibited bursting activity.

(B, E, and H) Percentage of neurons in each batch that exhibited bursting activity. Data shown as mean (± SEM).

(C and F) Mean firing rate in neurons that did not exhibit bursting activity.

Statistics: (A) Welch's *t* test. *n* = 546 (CTRL3) and 532 (MAP1B-EE) neurons.

(B) Unpaired *t* test. *n* = 3 independent batches of differentiation (B1–B3).

(C) Brown-Forsythe & Welch's ANOVA with Dunnett's T3 correction for multiple comparisons. *n* = 32 (CTRL1), 145 (FXS1+shNC), and 79 (FXS1+shMAP1B) neurons.

(legend continued on next page)

by SAMS, particularly after validation of the Flagged Electrodes lists, is particularly significant in the context of high-content screening using MEA plates in 48- or 96-well plate formats, as these features dramatically reduce the amount of time the user will need to spend checking electrodes before they obtain their final results. The application of SAMS to existing MEA datasets demonstrates its practical utility in various research scenarios. This versatility makes SAMS a valuable tool for a wide range of neuroscience applications, from basic research to disease modeling and drug discovery.

While SAMS was developed for the Axion platform, its core algorithms (HDT, DTW, and spectral clustering) are platform-agnostic. Adaptation to other low-density MEA systems such as Multi Channel Systems would primarily require data interface modifications rather than algorithmic changes and could be implemented in a future version.

Limitations of this study

It is important to note that this first iteration of SAMS, like most other available spike sorting algorithms and platforms, has limitations. SAMS was developed to aid spike sorting, but it is not a solution to all issues that users may encounter. It is essential that users verify and correct any incorrect sorts before drawing conclusions about their data. One limitation is that the algorithm's performance at the default settings appears to decrease with very high spike counts per electrode, suggesting potential room for improvement in handling highly active neurons or high-noise scenarios. Oversorting can occur when spikes are triggered by double thresholding or time shifts, resulting in separate clusters that represent the same neuron. If the waveforms are not similar enough to be detected by DTW as originating from the same unit, they remain split. Undersorting happens when waveforms from different neurons differ only slightly, causing substantial overlap in PCA space, or due to waveform similarities between units or noise contamination that shifts a spike's position in feature space toward a neighboring cluster. It appears as a small cluster hidden within a larger one in the PCA projection, making it difficult to distinguish separate units. As should be done with all new methods, we recommend that users first perform a pilot analysis comparing SAMS to ground truth data so they can determine the settings that work best for their data. We also recommend validation of key findings using complementary methods of measuring single neuron electrical activity, such as patch clamp recording or calcium imaging. All sorts should also be user-verified before drawing conclusions. Future iterations of SAMS may also incorporate machine learning techniques to further refine its performance in these edge cases. Additionally, this current iteration of SAMS cannot identify or define network bursts at the single unit level; therefore, network activity data currently still need to be examined on an electrode-to-electrode basis. This version of SAMS only reports electrode-level network spiking and bursting metrics, as well as the synchrony index; therefore, other measures of synchrony such as area under normalized cross-correlation still need to be acquired through standard bulk MEA analysis. SAMS was developed using MATLAB, a computationally heavy language that can affect performance speed depending on existing hardware. Implementation of SAMS in the future using lower-level languages such as C could increase processing speed. Finally, the data files used for the development of SAMS almost exclusively consisted of cortical excitatory neurons that were cultured for only up to 8 weeks *in vitro*, so analysis of recordings containing more electrically mature neurons, or those containing purely inhibitory or non-cortical neuronal subtypes may produce differences in the overall accuracy. The files used for the development and testing of SAMS shown here only contained data from neurons cultured on 96-well and 48-well MEA plates, which contain 8 and 16 electrodes, respectively, spaced at 350 μm. Since the electrode spacing is only slightly less in the higher-density plates offered by Axion (300 μm), we do not anticipate performance differences if SAMS were to be used on data from these types of plates. Therefore, as SAMS is applied to a broader variety of datasets, additional updates and refinements to the SAMS algorithm can be made to retain its high levels of accuracy. We encourage users to contact us and provide example datasets if they encounter recurring issues with over- or undersorting so that we can continue to further improve the SAMS algorithm and increase its functionality to meet the broader needs of the hPSC-derived neuron community.

(D) Brown-Forsythe & Welch's ANOVA with Dunnett's T3 correction for multiple comparisons. n = 26 (CTRL1), 80 (FXS1+shNC), and 116 (FXS1+shMAP1B) neurons.
(E) Unpaired t test. n = 3 independent batches of differentiation (B1–B3).
(F) Welch's t test. n = 98 (CTRL2) and 664 (FXS2) neurons.
(G) Welch's t test. n = 172 (CTRL2) and 103 (FXS2) neurons.
(H) Unpaired t test. n = 4 independent batches of differentiation (B1–B3 and B5). Batches are represented by different symbol shapes. $^{*}p < 0.05$, $^{**}p < 0.01$, $^{***}p < 0.005$, $^{****}p < 0.001$.
See also Figure S7.

Please cite this article in press as: Ren et al., A semi-automated MEA spike sorting method for high-throughput assessment of cultured neurons, Stem Cell Reports (2026), https://doi.org/10.1016/j.stemcr.2026.102872

METHODS

Generation of aligned spike files for spike sorting

Raw MEA data files were loaded into AxIS navigator software (Axion Biosystems). "Spontaneous" configuration with the Spike Detector set to "Peak Adaptive Threshold" was selected, while all other settings were set at the default values. The "Peak Adaptive Threshold" setting generates spike files that contain annotated spikes and burst information and aligned waveforms to facilitate spike sorting. The specific values for the Spike Detector settings are in Table S6. Each spike file was converted to the NeuroExplorer (.nex) format using Axion's Data Export Tool, so it was compatible with Plexon's OFS software.

Manual spike sorting of MEA data files to establish ground truth

Prior to assessing the accuracy of SAMS and OFS spike sorting algorithms, the data files to be used for this assessment were first manually analyzed in OFS to determine the number of units on each electrode in each data file. Each .nex file was loaded into OFS to enable viewing of unsorted aligned waveform shapes and waveform PCA data and manual sorting of waveforms into putative units. Detailed manual sorting process is provided in the supplemental methods. Briefly, PCA clustering and the peaks of aligned waveforms were used to define putative units, which were then subdivided into smaller subunits. These subunits were manually inspected to compare their similarity, and similar subunits were remerged into one unit. This process was performed in multiple iterations until a final set of units remained that were distinct from one another based on peak location, trough location, peak-to-trough amplitude, and waveform shape dissimilarity. Units with a firing rate below 0.1 Hz were excluded from the final unit count. All recorded electrodes in each batch of cells were included in the analysis.

SAMS

SAMS was optimized to handle the scale and characteristics of *in vitro* MEA data, where hundreds of electrodes must be analyzed. The key algorithmic components include PCA to project spike waveforms into lower dimension, then spectral clustering to assign initial units by evaluating K = 1–5 clusters. Best fit is chosen based on the Davies-Bouldin Index. To fix undersorting, Hartigan's dip test (HDT) is applied to flag clusters with multimodality in principal component distribution, which are then split accordingly. To fix oversorting, dynamic time warping (DTW) is applied to identify and merge units possessing similar waveform characteristics but temporally shifted. We also have quality control steps: waveforms that deviate more than three SDs from a unit's mean template are removed as outliers, spikes violating the refractory period (default: 1.5 ms) are discarded, and low firing rate units (default: 0.1 Hz) are excluded. SAMS also flags potentially missorted electrodes as possible multi-unit (PMU; failed HDT or low DTW distance) or over-excluded unit (OEU; excessive waveform exclusion) for manual review. Details are provided in the supplemental methods and Table S2 and can also be found on the SAMS GitHub.

SAMS and OFS accuracy assessment

To assess the accuracy of SAMS and OFS algorithms, the number of units identified on each electrode was compared to the number of units identified by manual spike sorting. SAMS was run using the default settings (Table S2). Four different automated spike sorting algorithms available in OFS software were first tested using the default parameters, then each parameter was adjusted individually from the default to determine whether it influenced the algorithm's accuracy and if so, whether the accuracy could be improved. The settings for each parameter tested are provided in Table S3. An electrode was classified as incorrectly "oversorted" when the number of units identified by an algorithm was greater than the number of units identified by manual spike sorting and considered incorrectly "undersorted" when the number of units identified by an algorithm was less than the number of units identified by manual spike sorting.

To more thoroughly assess the accuracy of SAMS, the PCA plots and waveform plots for each electrode were visually inspected to confirm whether waveforms appeared to be assigned to the correct units. Although uncommon, an electrode was classified as incorrectly "missorted" when the number of units identified by SAMS matched the number of units identified by manual spike sorting, but the assignment of waveforms was found to be incorrect upon user inspection. For simplicity of reporting, these units were counted as "undersorted" when calculating the types of errors committed by SAMS or OFS.

To avoid reporting an inflated estimate of SAMS' capabilities, we have reported accuracy as the percentage of electrodes that were completely sorted correctly, unless stated otherwise in the figure legend: an electrode was only considered "correct" if the number of units identified was correct and if the majority of the waveforms (greater than 90%) were assigned to the correct units. Otherwise, the entire electrode was categorized as "incorrect." Further, we also did not exclude any difficult-to-sort electrodes from any of the datasets.

MEA datasets

All MEA datasets used in this study were recorded from hPSC-derived excitatory neurons and were previously

published (Afshar-Saber et al., 2024b; Guo et al., 2023; Shen et al., 2023). For detailed batch information, including the number of active wells and electrodes, see Table S5. For detailed information on iPSC lines and neuronal differentiation protocols, see supplemental methods.

Data analysis and statistics

For detailed statistical information, see supplemental methods. Electrode diagram in Figure 5B was generated using MATLAB. Graphs plotting waveform number against SAMS accuracy were generated using R. Kendall's tau and bootstrapping analyses (Figures 5E, S6B, and S6D) were performed in R (https://github.com/Zhao-Lab-UW/SAMS-R-analyses/tree/main). Graphing and statistical analysis for all other figures was performed using Prism software (GraphPad).

RESOURCE AVAILABILITY

Lead contact

Requests for further information and resources should be directed to and will be fulfilled by the lead contact, Xinyu Zhao (xinyu.zhao@wisc.edu).

Materials availability

SAMS (RRID: SCR_027843) can be accessed at https://github.com/Zhao-Lab-UW/SAMS-Semi-Automatic-MEA-Spike-sorting-pipeline-. There was no unique reagent generated in this study.

Data and code availability

The code used for generating the figures and data files used in this study can be accessed at https://github.com/Zhao-Lab-UW/SAMS-Semi-Automatic-MEA-Spike-sorting-pipeline-. SAMS incorporates the following third-party components: AxionFileLoader (Axion BioSystems), Hartigan's dip test (translated by F. Mechler from Hartigan and Hartigan, 1985; Hartigan and Hartigan, 1985), and InterX (NS, 2025).

ACKNOWLEDGMENTS

We thank Drs. Wardiya Afshar-Saber and Mustafa Sahin for kindly sharing their MEA data and members of the Zhao lab for their helpful discussion. This work was supported by the DOD IIRA grant W81XWH-22-1-0621 (to X.Z.); National Institutes of Health (R01MH118827, R01MH116582, R01MH136152, and R01NS138268 to X.Z.; R01EY029438 and R01EY035005 to A.R.; P50HD105353 to Waisman Center; DP2NS122605 to A.H.; and P51OD011106 to A.R.); Retina Research Foundation Edwin and Dorothy Gamewell Professorship, McPherson Eye Research Institute (to A.R.), Kellett Mid-Career Award, Wisconsin Alumni Research Foundation, Jenni and Kyle Professorship, Vilas Distinguished Achievement Professorship, Eagle Autism Foundation, and Simons Foundation Autism Research Initiative (to X.Z.); postdoctoral fellowships from the Wisconsin Stem Cell and Regenerative Medicine Center (SCRMC), Fragile X Research Foundation (FRAXA), and the Autism Science Foundation (to C.L.S.); SciMed scholarships, T32 GM141013, and predoctoral fellowship from the SCRMC (to N.M.M.-A.).

AUTHOR CONTRIBUTIONS

C.L.S. and X.Z. conceived the concept and designed the study. X.R. developed the method with help from A.R., R.C.D., and A.H. C.L.S., X.R., and E.E.D. performed accuracy checking and created figures and tables. N.M.M.-A. created the logo and graphical abstract. X.R., C.L.S., and X.Z. wrote the manuscript. All authors edited the manuscript.

DECLARATION OF INTERESTS

The authors declare no competing interests.

SUPPLEMENTAL INFORMATION

Supplemental information can be found online at https://doi.org/10.1016/j.stemcr.2026.102872.

Received: January 20, 2025
Revised: March 1, 2026
Accepted: March 2, 2026

REFERENCES

Afshar-Saber, W., Chen, C., Teaney, N.A., Kim, K., Yang, Z., Gasparoli, F.M., Ebrahimi-Fakhari, D., Buttermore, E.D., Pin-Fang Chen, I., Pearl, P.L., and Sahin, M. (2024). Generation and characterization of six human induced pluripotent stem cell lines (hiPSCs) from three individuals with SSADH Deficiency and CRISPR-corrected isogenic controls. Stem Cell Res. *77*, 103424. https://doi.org/10.1016/j.scr.2024.103424.

Afshar-Saber, W., Teaney, N.A., Winden, K.D., Jumo, H., Shi, X., McGinty, G., Hubbs, J., Chen, C., Tokatly Latzer, I., Gasparoli, F., et al. (2024). ALDH5A1-deficient iPSC-derived excitatory and inhibitory neurons display cell type specific alterations. Neurobiol. Dis. *190*, 106386. https://doi.org/10.1016/j.nbd.2023.106386.

Amatya, D.N., Linker, S.B., Mendes, A.P.D., Santos, R., Erikson, G., Shokhirev, M.N., Zhou, Y., Sharpee, T., Gage, F.H., Marchetto, M. C., and Kim, Y. (2019). Dynamical Electrical Complexity Is Reduced during Neuronal Differentiation in Autism Spectrum Disorder. Stem Cell Rep. *13*, 474–484. https://doi.org/10.1016/j.stemcr.2019.08.001.

Anderson, N.C., Chen, P.F., Meganathan, K., Afshar Saber, W., Petersen, A.J., Bhattacharyya, A., Kroll, K.L., and Sahin, M.; Cross-IDDRC Human Stem Cell Working Group (2021). Balancing serendipity and reproducibility: Pluripotent stem cells as experimental systems for intellectual and developmental disorders. Stem Cell Rep. *16*, 1446–1457. https://doi.org/10.1016/j.stemcr.2021.03.025.

Buccino, A.P., Hurwitz, C.L., Garcia, S., Magland, J., Siegle, J.H., Hurwitz, R., and Hennig, M.H. (2020). SpikeInterface, a unified framework for spike sorting. eLife *9*, e61834. https://doi.org/10.7554/eLife.61834.

Cao, Y., Rakhilin, N., Gordon, P.H., Shen, X., and Kan, E.C. (2016). A real-time spike classification method based on dynamic time warping for extracellular enteric neural recording with large waveform variability. J. Neurosci. Methods *261*, 97–109. https://doi.org/10.1016/j.jneumeth.2015.12.006.

Carlson, D., and Carin, L. (2019). Continuing progress of spike sorting in the era of big data. Curr. Opin. Neurobiol. *55*, 90–96. https://doi.org/10.1016/j.conb.2019.02.007.

Choi, J.S., Lee, H.J., Rajaraman, S., and Kim, D.H. (2021). Recent advances in three-dimensional microelectrode array technologies for in vitro and in vivo cardiac and neuronal interfaces. Biosens. Bioelectron. *171*, 112687. https://doi.org/10.1016/j.bios.2020.112687.

Cotterill, E., Charlesworth, P., Thomas, C.W., Paulsen, O., and Eglen, S.J. (2016). A comparison of computational methods for detecting bursts in neuronal spike trains and their application to human stem cell-derived neuronal networks. J. Neurophysiol. *116*, 306–321. https://doi.org/10.1152/jn.00093.2016.

Das Sharma, S., Pal, R., Reddy, B.K., Selvaraj, B.T., Raj, N., Samaga, K.K., Srinivasan, D.J., Ornelas, L., Sareen, D., Livesey, M.R., et al. (2020). Cortical neurons derived from human pluripotent stem cells lacking FMRP display altered spontaneous firing patterns. Mol. Autism *11*, 52. https://doi.org/10.1186/s13229-020-00351-4.

Gildin, L., Rauti, R., Vardi, O., Kuznitsov-Yanovsky, L., Maoz, B.M., Segal, M., and Ben-Yosef, D. (2022). Impaired Functional Connectivity Underlies Fragile X Syndrome. Int. J. Mol. Sci. *23*, 2048. https://doi.org/10.3390/ijms23042048.

Graef, J.D., Wu, H., Ng, C., Sun, C., Villegas, V., Qadir, D., Jesseman, K., Warren, S.T., Jaenisch, R., Cacace, A., and Wallace, O. (2020). Partial FMRP expression is sufficient to normalize neuronal hyperactivity in Fragile X neurons. Eur. J. Neurosci. *51*, 2143–2157. https://doi.org/10.1111/ejn.14660.

Guan, S., Tian, H., Yang, Y., Liu, M., Ding, J., Wang, J., and Fang, Y. (2023). Self-assembled ultraflexible probes for long-term neural recordings and neuromodulation. Nat. Protoc. *18*, 1712–1744. https://doi.org/10.1038/s41596-023-00824-9.

Guo, Y., Shen, M., Dong, Q., Méndez-Albelo, N.M., Huang, S.X., Sirois, C.L., Le, J., Li, M., Jarzembowski, E.D., Schoeller, K.A., et al. (2023). Elevated levels of FMRP-target MAP1B impair human and mouse neuronal development and mouse social behaviors via autophagy pathway. Nat. Commun. *14*, 3801. https://doi.org/10.1038/s41467-023-39337-0.

Hartigan, J.A., and Hartigan, P.M. (1985). The Dip Test of Unimodality. Ann. Statist. *13*, 70–84.

Hruska-Plochan, M., Wiersma, V.I., Betz, K.M., Mallona, I., Ronchi, S., Maniecka, Z., Hock, E.M., Tantardini, E., Laferriere, F., Sahadevan, S., et al. (2024). A model of human neural networks reveals NPTX2 pathology in ALS and FTLD. Nature *626*, 1073–1083. https://doi.org/10.1038/s41586-024-07042-7.

Hulme, A.J., Maksour, S., St-Clair Glover, M., Miellet, S., and Dottori, M. (2022). Making neurons, made easy: The use of Neurogenin-2 in neuronal differentiation. Stem Cell Rep. *17*, 14–34. https://doi.org/10.1016/j.stemcr.2021.11.015.

Hyvärinen, T., Hyysalo, A., Kapucu, F.E., Aarnos, L., Vinogradov, A., Eglen, S.J., Ylä-Outinen, L., and Narkilahti, S. (2019). Functional characterization of human pluripotent stem cell-derived cortical networks differentiated on laminin-521 substrate: comparison to rat cortical cultures. Sci. Rep. *9*, 17125. https://doi.org/10.1038/s41598-019-53647-8.

Jun, J.J., Steinmetz, N.A., Siegle, J.H., Denman, D.J., Bauza, M., Barbarits, B., Lee, A.K., Anastassiou, C.A., Andrei, A., Aydın, Ç., et al. (2017). Fully integrated silicon probes for high-density recording of neural activity. Nature *551*, 232–236. https://doi.org/10.1038/nature24636.

Kiskinis, E., Sandoe, J., Williams, L.A., Boulting, G.L., Moccia, R., Wainger, B.J., Han, S., Peng, T., Thams, S., Mikkilineni, S., et al. (2014). Pathways disrupted in human ALS motor neurons identified through genetic correction of mutant SOD1. Cell Stem Cell *14*, 781–795. https://doi.org/10.1016/j.stem.2014.03.004.

Lemieux, M.R., Freigassner, B., Hanson, J.L., Thathey, Z., Opp, M. R., Hoeffer, C.A., and Link, C.D. (2024). Multielectrode array characterization of human induced pluripotent stem cell derived neurons in co-culture with primary human astrocytes. PLoS One *19*, e0303901. https://doi.org/10.1371/journal.pone.0303901.

Li, M., Shin, J., Risgaard, R.D., Parries, M.J., Wang, J., Chasman, D., Liu, S., Roy, S., Bhattacharyya, A., and Zhao, X. (2020). Identification of FMR1-regulated molecular networks in human neurodevelopment. Genome Res. *30*, 361–374. https://doi.org/10.1101/gr.251405.119.

Lin, H.C., He, Z., Ebert, S., Schörnig, M., Santel, M., Nikolova, M.T., Weigert, A., Hevers, W., Kasri, N.N., Taverna, E., et al. (2021). NGN2 induces diverse neuron types from human pluripotency. Stem Cell Rep. *16*, 2118–2127. https://doi.org/10.1016/j.stemcr.2021.07.006.

Liu, H., Lu, J., Chen, H., Du, Z., Li, X.J., and Zhang, S.C. (2015). Spinal muscular atrophy patient-derived motor neurons exhibit hyperexcitability. Sci. Rep. *5*, 12189. https://doi.org/10.1038/srep12189.

Liu, X.S., Wu, H., Krzisch, M., Wu, X., Graef, J., Muffat, J., Hnisz, D., Li, C.H., Yuan, B., Xu, C., et al. (2018). Rescue of Fragile X Syndrome Neurons by DNA Methylation Editing of the FMR1 Gene. Cell *172*, 979–992.e6. https://doi.org/10.1016/j.cell.2018.01.012.

Liu, Y., Yao, X., Fan, C., Zhang, G., Luo, X., and Qian, Y. (2023). Microfabrication and lab-on-a-chip devices promotein vitromodeling of neural interfaces for neuroscience researches and preclinical applications. Biofabrication *16*. https://doi.org/10.1088/1758-5090/ad032a.

Lv, S., He, E., Luo, J., Liu, Y., Liang, W., Xu, S., Zhang, K., Yang, Y., Wang, M., Song, Y., et al. (2023). Using Human-Induced Pluripotent Stem Cell Derived Neurons on Microelectrode Arrays to Model Neurological Disease: A Review. Adv. Sci. *10*, e2301828. https://doi.org/10.1002/advs.202301828.

Mayer, M., Arrizabalaga, O., Lieb, F., Ciba, M., Ritter, S., and Thielemann, C. (2018). Electrophysiological investigation of human embryonic stem cell derived neurospheres using a novel spike detection algorithm. Biosens. Bioelectron. *100*, 462–468. https://doi.org/10.1016/j.bios.2017.09.034.

McCready, F.P., Gordillo-Sampedro, S., Pradeepan, K., Martinez-Trujillo, J., and Ellis, J. (2022). Multielectrode Arrays for Functional Phenotyping of Neurons from Induced Pluripotent Stem Cell Models of Neurodevelopmental Disorders. Biology *11*, 316. https://doi.org/10.3390/biology11020316.

Mehta, S.R., Tom, C.M., Wang, Y., Bresee, C., Rushton, D., Mathkar, P.P., Tang, J., and Mattis, V.B. (2018). Human Huntington's Disease iPSC-Derived Cortical Neurons Display Altered Transcriptomics, Morphology, and Maturation. Cell Rep. *25*, 1081–1096.e6. https://doi.org/10.1016/j.celrep.2018.09.076.

Mohammadi, Z., Denman, D.J., Klug, A., and Lei, T.C. (2024). A fully automatic multichannel neural spike sorting algorithm with spike reduction and positional feature. J. Neural. Eng. *21*, 046039. https://doi.org/10.1088/1741-2552/ad647d.

Mossink, B., Verboven, A.H.A., van Hugte, E.J.H., Klein Gunnewiek, T.M., Parodi, G., Linda, K., Schoenmaker, C., Kleefstra, T., Kozicz, T., van Bokhoven, H., et al. (2021). Human neuronal networks on micro-electrode arrays are a highly robust tool to study disease-specific genotype-phenotype correlations in vitro. Stem Cell Rep. *16*, 2182–2196. https://doi.org/10.1016/j.stemcr.2021.07.001.

Napoli, A., and Obeid, I. (2016). Comparative Analysis of Human and Rodent Brain Primary Neuronal Culture Spontaneous Activity Using Micro-Electrode Array Technology. J. Cell. Biochem. *117*, 559–565. https://doi.org/10.1002/jcb.25312.

Negri, J., Menon, V., and Young-Pearse, T.L. (2020). Assessment of Spontaneous Neuronal Activity In Vitro Using Multi-Well Multi-Electrode Arrays: Implications for Assay Development. eNeuro *7*. https://doi.org/10.1523/eneuro.0080-19.2019.

Niu, W., and Parent, J.M. (2020). Modeling genetic epilepsies in a dish. Dev. Dyn. *249*, 56–75. https://doi.org/10.1002/dvdy.79.

NS (2025). Curve Intersections (MATLAB Central File Exchange).

Obaid, A., Hanna, M.E., Wu, Y.W., Kollo, M., Racz, R., Angle, M.R., Müller, J., Brackbill, N., Wray, W., Franke, F., et al. (2020). Massively parallel microwire arrays integrated with CMOS chips for neural recording. Sci. Adv. *6*, eaay2789. https://doi.org/10.1126/sciadv.aay2789.

Pradeepan, K.S., McCready, F.P., Wei, W., Khaki, M., Zhang, W., Salter, M.W., Ellis, J., and Martinez-Trujillo, J. (2024). Calcium-Dependent Hyperexcitability in Human Stem Cell-Derived Rett Syndrome Neuronal Networks. Biol. Psychiatry Glob. Open Sci. *4*, 100290. https://doi.org/10.1016/j.bpsgos.2024.100290.

Que, Z., Olivero-Acosta, M.I., Zhang, J., Eaton, M., Tukker, A.M., Chen, X., Wu, J., Xie, J., Xiao, T., Wettschurack, K., et al. (2021). Hyperexcitability and Pharmacological Responsiveness of Cortical Neurons Derived from Human iPSCs Carrying Epilepsy-Associated Sodium Channel Nav1.2-L1342P Genetic Variant. J. Neurosci. *41*, 10194–10208. https://doi.org/10.1523/jneurosci.0564-21.2021.

Rosa, F., Dhingra, A., Uysal, B., Mendis, G.D.C., Loeffler, H., Elsen, G., Mueller, S., Schwarz, N., Castillo-Lizardo, M., Cuddy, C., et al. (2020). In Vitro Differentiated Human Stem Cell-Derived Neurons Reproduce Synaptic Synchronicity Arising during Neurodevelopment. Stem Cell Rep. *15*, 22–37. https://doi.org/10.1016/j.stemcr.2020.05.015.

Sandoval, S.O., Méndez-Albelo, N.M., Xu, Z., and Zhao, X. (2024). From wings to whiskers to stem cells: why every model matters in fragile X syndrome research. J. Neurodev. Disord. *16*, 30. https://doi.org/10.1186/s11689-024-09545-w.

Shen, M., Sirois, C.L., Guo, Y., Li, M., Dong, Q., Méndez-Albelo, N.M., Gao, Y., Khullar, S., Kissel, L., Sandoval, S.O., et al. (2023). Species-specific FMRP regulation of RACK1 is critical for prenatal cortical development. Neuron *111*, 3988–4005.e11. https://doi.org/10.1016/j.neuron.2023.09.014.

Souza, B.C., Lopes-Dos-Santos, V., Bacelo, J., and Tort, A.B.L. (2019). Spike sorting with Gaussian mixture models. Sci. Rep. *9*, 3627. https://doi.org/10.1038/s41598-019-39986-6.

Spira, M.E., and Hai, A. (2013). Multi-electrode array technologies for neuroscience and cardiology. Nat. Nanotechnol. *8*, 83–94. https://doi.org/10.1038/nnano.2012.265.

Tidball, A.M., Lopez-Santiago, L.F., Yuan, Y., Glenn, T.W., Margolis, J.L., Clayton Walker, J., Kilbane, E.G., Miller, C.A., Martina Bebin, E., Scott Perry, M., et al. (2020). Variant-specific changes in persistent or resurgent sodium current in SCN8A-related epilepsy patient-derived neurons. Brain *143*, 3025–3040. https://doi.org/10.1093/brain/awaa247.

Tyssowski, K.M., Letai, K.C., Rendall, S.D., Tan, C., Nizhnik, A., Kaeser, P.S., and Gray, J.M. (2019). Firing Rate Homeostasis Can Occur in the Absence of Neuronal Activity-Regulated Transcription. J. Neurosci. *39*, 9885–9899. https://doi.org/10.1523/jneurosci.1108-19.2019.

Vatine, G.D., Al-Ahmad, A., Barriga, B.K., Svendsen, S., Salim, A., Garcia, L., Garcia, V.J., Ho, R., Yucer, N., Qian, T., et al. (2017). Modeling Psychomotor Retardation using iPSCs from MCT8-Deficient Patients Indicates a Prominent Role for the Blood-Brain Barrier. Cell Stem Cell *20*, 831–843.e5. https://doi.org/10.1016/j.stem.2017.04.002.

Vertkin, I., Styr, B., Slomowitz, E., Ofir, N., Shapira, I., Berner, D., Fedorova, T., Laviv, T., Barak-Broner, N., Greitzer-Antes, D., et al. (2015). GABAB receptor deficiency causes failure of neuronal homeostasis in hippocampal networks. Proc. Natl. Acad. Sci. USA *112*, E3291–E3299. https://doi.org/10.1073/pnas.1424810112.

von Luxburg, U. (2007). A tutorial on spectral clustering. Stat. Comput. *17*, 395–416. https://doi.org/10.1007/s11222-007-9033-z.

Wang, R., Xu, Y., Zhang, Y., Hu, X., Li, Y., and Zhang, S. (2023). A Fast and Effective Spike Sorting Method Based on Multi-Frequency Composite Waveform Shapes. Brain Sci. *13*, 1156. https://doi.org/10.3390/brainsci13081156.

Zhang, H., Rong, G., Bian, S., and Sawan, M. (2022). Lab-on-Chip Microsystems for Ex Vivo Network of Neurons Studies: A Review. Front. Bioeng. Biotechnol. *10*, 841389. https://doi.org/10.3389/fbioe.2022.841389.

Zhao, X., and Bhattacharyya, A. (2018). Human Models Are Needed for Studying Human Neurodevelopmental Disorders. Am. J. Hum. Genet. *103*, 829–857. https://doi.org/10.1016/j.ajhg.2018.10.009.